(Received 25 June 2024, Accepted 5 September 2024, Scheduled 19 September 2024)

Double and Triple-Vector Hybrid Modulation Model Predictive Control Based on Virtual Synchronous Generator

Yang Zhang[1], Yuwei Meng[1], Xiuhai Yang[1], Kun Cao[1], Sai Zhang[1], and Zhun Cheng[2,*]

[1]*Hunan University of Technology, Zhuzhou 412007, China*
[2]*Hunan Railway Professional Technology College, Zhuzhou 412001, China*

ABSTRACT: To address the issues of high current harmonic and power ripple in the traditional Finite Control Set Model Predictive Control (FCS-MPC) strategy for virtual synchronous generator system with quasi-Z-source inverter (qZSI-VSG), a double and triple-vector hybrid modulation model predictive control strategy is proposed. This strategy utilizes the inductor current sub-cost function to select the shoot-through state (ST state) or the non-shoot-through state (NST state). When NST state is selected, the voltage vector combinations in the double-vector and the triple-vector are initially established. Then, the voltage vector combinations are reduced from 18 groups to 6 groups by using the vector combination quick selection table. Subsequently, the duty cycle of each voltage vector is then determined based on the value of its cost function, and the voltage vector is re-synthesized. Finally, the predicted values of all control variables are calculated and substituted into the cost function for optimization. Experimental results show that the proposed strategy reduces 48.62% of current harmonic, 50% of active power ripple, and 25.53% of capacitor voltage ripple compared to the traditional strategy, which effectively improves the system control performance.

1. INTRODUCTION

Virtual Synchronous Generator (VSG) [1] not only simulates the external characteristics of traditional synchronous generators, but also performs active power frequency and reactive power voltage control. Among them, active power frequency control can simulate the inertia and damping features of synchronous generators [2, 3]. Compared with the traditional grid-connected inverter, when distributed energy sources are connected to the grid on a large scale, VSG can effectively mitigate the impact that they have on the grid, improve the reactive power compensation and voltage support capacity of the system, and thereby enhance the compatibility between the grid-connected inverter and the grid.

Quasi-Z-source inverter (qZSI), as a novel inverter topology, is characterized by a wide voltage input range and the ability of voltage boosting and bucking [4]. It has the advantages of no need to set the dead time, allowing direct connection of the bridge arm, continuous input current, high efficiency, and high reliability [5–7]. However, when the new energy is connected to the grid by qZSI, the lack of inertia will lead to a reduction in the inertia of the power system. Therefore, the combination of qZSI and VSG can not only enhance the boosting ability and increase the inertia of the power system, but also eliminate the low-frequency torque ripple caused by the dead time in traditional voltage source inverters [8, 9], thereby improving the grid-connection stability of distributed generation systems.

Model Predictive Control (MPC) has significant advantages such as flexible control, simple implementation, rapid dynamic response, and no need to rely on PI controllers and PWM. As a result, MPC has been widely used and recognized in many fields such as power electronics, new energy, and motor drives [10, 11]. Refs. [12, 13] apply FCS-MPC to qZSI, and [14] takes VSG power control as the outer loop and adopts MPC in the inner loop to replace the traditional linear control. However, only a single voltage vector is used for each sampling cycle, which can lead to large system current harmonic and power ripple. Though it can be decreased by increasing the sampling frequency of the predictive control, the sampling frequency is restricted by the computational volume of the control algorithm.

In [15, 16], voltage source inverters use double-vector MPC strategies that utilize two voltage vectors at each sampling period to optimize the current control. Refs. [17, 18] propose triple-vector MPC strategies for PWM rectifiers and PMSM, which selects three voltage vectors at each sampling period, which can further reduce current ripple and torque ripple in PMSM. While the above multi-vector model predictive control approach helps to improve control performance, it also suffers from problems such as large computational volume. In order to realize multi-vector model predictive control and reduce the computational effort, a modulation model predictive control strategy (M^2PC) has been proposed and investigated in [19, 20]. Different from [15–18], the method proposed in [19, 20] determines the duty cycle of each voltage vector based on its cost function value, where the duty cycle is inversely related to the cost function value, and such calculation methods have the advantages of easy realization, small computational burden, and no over-modulation, and therefore it is used extensively in the area of matrix converter [21] and active power filter [22] control. Many scholars have verified the effectiveness of the modu-

* Corresponding author: Zhun Cheng (120277982@qq.com).

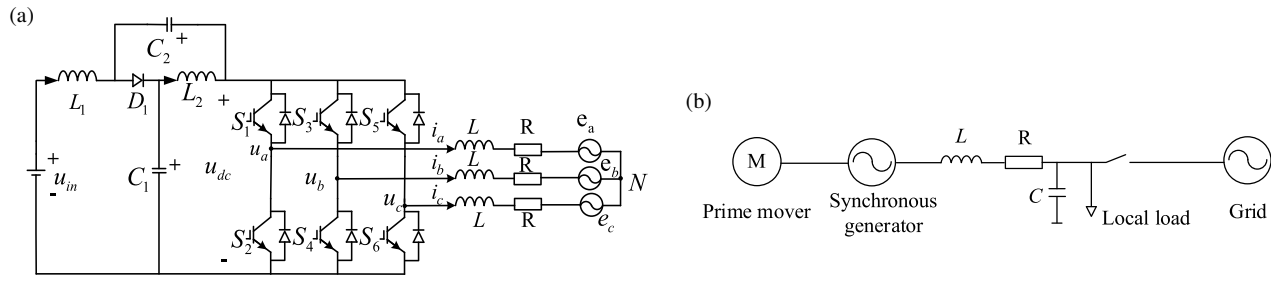

FIGURE 1. qZSI-VSG system. (a) qZSI main circuit diagram. (b) VSG basic topology equivalent diagram.

lation model predictive control strategy through simulation and experiments. In a qZSI-VSG system, there are multi-objective control demands such as inductor current, capacitor voltage, and output current, and the question of whether the optimal control can still be achieved by using the multi-vector model predictive control has rarely been studied.

In summary, to minimize the current harmonic and power ripple of the FCS-MPC strategy, a double and triple-vector hybrid modulation model predictive control (DTVH-M^{2}PC) strategy is proposed. The strategy effectively reduces the current harmonic and power ripple with better steady-state performance. The main contributions of this study are:

1) The inductor current sub-cost function is used to choose between shoot-through state (ST state) and the non-shoot-through state (NST state), reducing the complexity of calculating the vector duty cycle and simplifying the cost function.

2) The double-vector M^{2}PC (DV-M^{2}PC) strategy and triple-vector M^{2}PC (TV-M^{2}PC) strategy construct the cost functions about the capacitor voltage and the current under the NST state, and the duty cycle of each voltage vector is then determined based on its cost function value, where the duty cycle is inversely related to the cost function value. The control of multiple targets under the multi-vector control strategy is realized, and the control performance and computational simplicity of multiple targets are guaranteed.

3) Combining the DV-M^{2}PC and TV-M^{2}PC strategies, DTVH-M^{2}PC strategy is proposed, aiming to reduce redundancy in translation, which enriches the set of voltage vectors, improves the control accuracy, and reduces the computation with the vector combination quick selection table.

2. QZSI-VSG SYSTEM PRINCIPLE

VSG can provide inertia to grid-connected systems, while qZSI is characterized by its high boost capability and the absence of a required dead time. Combining the advantages of both, this paper constructs a qZSI-VSG system aimed at enhancing the performance and stability of grid integration. The main circuit of the qZSI, as shown in Figure 1(a), primarily includes a DC power source (u_{in}), a quasi-Z-source network, an inverter bridge, equivalent filter inductors (L), equivalent resistors (R), and the power grid.

As shown in Figure 1(b), the VSG corresponds to the conventional synchronous generator model, and the DC power source and quasi-Z source network are regarded as the prime mover. The voltage and current at the midpoint of the inverter are equivalent to the synchronous generator's internal potential and stator current, respectively, and L and R are equivalent to the synchronous reactance and stator armature resistance of the synchronous generator. The filtered output voltage is equivalent to the machine-end output voltage.

2.1. Working Principle and Mathematical Model of QZSI

qZSI realizes inductor and capacitor charging and discharging control by switching the three-phase bridge arms in different states, so that the DC chain voltage is pumped up in the NST state of the inverter bridge for boosting purposes. The simplified space vectors of the output voltage for eight switching combinations are given in Table 1.

TABLE 1. Switching status of QZSI.

Switching state	Output voltage	S_1	S_3	S_5	S_2	S_4	S_6
NST state	u_0	0	0	0	1	1	1
	u_1	1	0	0	0	1	1
	u_2	1	1	0	0	0	1
	u_3	0	1	0	1	0	1
	u_4	0	1	1	1	0	0
	u_5	0	0	1	1	1	0
	u_6	1	0	1	0	1	0
	u_7	1	1	1	0	0	0
ST state	u_8	1	1	1	1	1	1

The eight output voltage vectors of qZSI are:

$$u_x = \frac{2u_{dc}}{3}\left(S_A + aS_B + a^2 S_C\right) \tag{1}$$

where u_{dc} is the DC chain voltage; $a = e^{j2\pi/3}$; $x = [0, 1, 2, 3, 4, 5, 6, 7]$; S_A, S_B, and S_C are the switching states of phases A, B, and C, respectively. The predicted value of the output current is obtained from Figure 1:

$$i_{(\alpha,\beta)}(k+1) = \left(1 - \frac{RT_s}{L}\right) i_{(\alpha,\beta)}(k) + \frac{T_s}{L}\left(u_{(\alpha,\beta)}(k) - e_{(\alpha,\beta)}(k)\right) \tag{2}$$

where $i_{(\alpha,\beta)}(k)$, $u_{(\alpha,\beta)}(k)$, and $e_{(\alpha,\beta)}(k)$ are the output current, output voltage, and grid voltage components of the kth

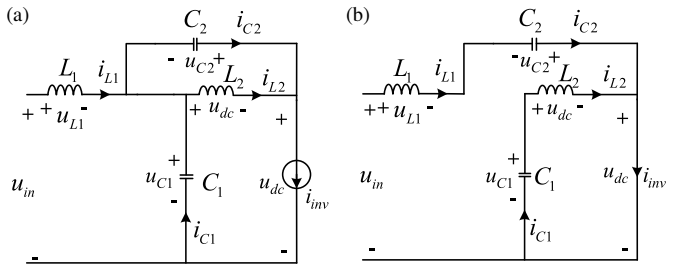

FIGURE 2. DC side equivalent circuit. (a) NST state. (b) ST state.

sampling period on the $\alpha\beta$ coordinate system; $i_{(\alpha,\beta)}(k+1)$ is the predicted output current component of the $k+1$th sampling period on the $\alpha\beta$ coordinate system; and T_s is the sampling period.

The qZSI has both ST and NST states of operation as shown in Figure 2. In the NST state, the input voltage u_{in} and inductors L_1 and L_2 supply the load and capacitor C_1 and C_2, and diode D_1 conducts. At this time the inductor current and capacitor voltage are predicted:

$$\begin{cases} i_{L1}(k+1) = \frac{T_s}{L_1}\left[u_{in}(k) - u_{C1}(k)\right] + i_{L1}(k) \\ u_{C1}(k+1) = u_{C1}(k) + \frac{T_s}{C_1}\left[i_{L1}(k) - i_{inv}(k)\right] \end{cases} \tag{3}$$

where L_1 and C_1 are the inductance and capacitance values in the impedance network; i_{L1} and u_{C1} are the inductance current and capacitance voltage, respectively; i_{inv} is the input current of the DC side of the inverter circuit, which can be calculated from the sampled three-phase currents $i_A(k)$, $i_B(k)$, and $i_C(k)$ at the kth sampling moment and combined with the switching states S_A, S_B, and S_C. This relationship is expressed as $i_{inv}(k) = i_A(k)S_A + i_B(k)S_B + i_C(k)S_C$.

In the ST state, the capacitors C_1 and C_2 discharge; the inductors L_1 and L_2 charge; D_1 is subjected to a reverse voltage and turned off; the upper and lower switching tubes of at least one bridge arm conduct simultaneously; and the load is shorted. The predicted values of inductor current and capacitor voltage at this time are:

$$\begin{cases} i_{L1}(k+1) = \frac{T_s}{L_1} u_{C1}(k) + i_{L1}(k) \\ u_{C1}(k+1) = u_{C1}(k) - \frac{T_s}{C_1} i_{L1}(k) \end{cases} \tag{4}$$

2.2. Virtual Synchronous Generator Control Principle

Synchronous generator rotor has a degree of inertia that suppresses short-term sudden changes in grid frequency. VSG introduces synchronous generator inertia and damping link into distributed inverter power supply control strategy by simulating the output characteristics of synchronous generator, and its active power control equation is:

$$J(\mathrm{d}\omega/\mathrm{d}t) = ((P_{ref} - P_e)/\omega_g) - D(\omega - \omega_g) \tag{5}$$

where ω is the VSG electrical angular velocity; ω_g is the grid synchronous electrical angular velocity; J is the rotor moment of inertia of the VSG; D is the damping coefficient of the VSG; P_{ref} is the reference value of the active power; P_e is the output active power. The VSG active power control is shown in Figure 3.

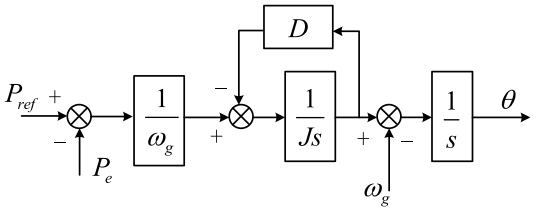

FIGURE 3. Block diagram of VSG active power control.

In a synchronous generator, the adjustment of the generator terminal voltage and reactive power output is achieved by adjusting the excitation current. Similarly, the VSG realizes the adjustment of terminal voltage and reactive power by adjusting its virtual potential E_m. The VSG reactive power voltage control equation is:

$$E_m = E_0 + \left[Q_{ref} - Q_e + k_q(U_{cn} - U_c)\right]/k_i s \tag{6}$$

where Q_{ref} is the reference value of reactive power; Q_e is the output reactive power; k_q is the reactive voltage sag coefficient; $1/k_i$ is the integrator gain; E_o is the no-load electromotive force; U_{cn} is the nominal value of the machine terminal voltage; U_c is the actual output value of the machine terminal voltage. The reactive power control of VSG is shown in Figure 4.

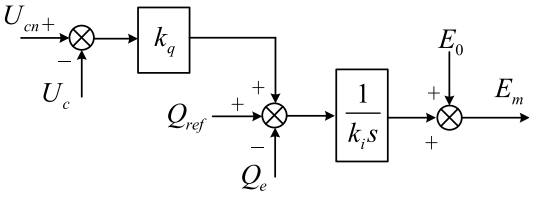

FIGURE 4. Block diagram of VSG reactive power control.

3. DTVH-M^{2}PC STRATEGY FOR QZSI-VSG SYSTEM

To address the problems of large current harmonic and power ripple in FCS-MPC, the DTVH-M^{2}PC strategy for qZSI-VSG system is proposed. Firstly, the cost function is reset to reduce the number of weights and to facilitate the calculation of the duty cycle of multiple vectors; then use the value of the cost function of each voltage vector to calculate its duty cycle in the DV-M^{2}PC and TV-M^{2}PC strategy, which reduces the current harmonic and power ripple; finally, the DTVH-M^{2}PC strategy is proposed to achieve further optimization by combining the DV-M^{2}PC and TV-M^{2}PC strategy.

3.1. Setting of the Cost Function

The cost function in the FCS-MPC strategy has three weight coefficients, and there exists the problem that it is difficult to adjust the weight coefficients more than one, so it is necessary to reset the cost function. qZSI is in the NST state, and the inductor current decreases; in the ST state, the inductor current increases. Based on this characterization, this paper first determines whether the next sampling period is in the ST state according to the predicted value of inductor current, and the

sub-cost function of this algorithm is:

$$g_{iL1} = |i_{L1\_ref} - i_{L1\_ST}(k+1)| - |i_{L1\_ref} - i_{L1\_NST}(k+1)| \quad (7)$$

where $i_{L1\_ST}(k+1)$ and $i_{L1\_NST}(k+1)$ are the predicted values of the inductor current in the ST state and NST state for the $(k+1)$th sampling period, respectively.

$$g = [i_{\alpha\_ref} - i_{\alpha}(k+1)]^2 + [i_{\beta\_ref} - i_{\beta}(k+1)]^2 + \lambda [u_{C1\_ref}(k) - u_{C1}(k+1)]^2 \quad (8)$$

where i_{α_ref} and i_{β_ref} are the components of the output current reference value in the $\alpha\beta$ coordinate system; $u_{C1\_ref}(k)$ is the capacitance voltage reference value; and λ is the weighting coefficient of the capacitance voltage. If the next control cycle is a ST state according to (7), the ST voltage vector is output directly. If it is an NST state, the cost function of output current and capacitor voltage in (8) is calculated, and the voltage vector that minimizes the cost function is selected.

3.2. Duty Cycle Calculation

In double-vector and triple-vector model predictive control strategies, in order to obtain the synthesized voltage vectors, the duty cycle of the vectors during a sampling period should be calculated first. Since the system has a very high sampling frequency, the weighted error of each voltage vector during a sampling period is approximated as:

$$\mathcal{E}_j = \{e_{ij}d_{ij} | i \in R_j\} \quad (9)$$

where e_{ij} is the error at the jth voltage vector of the ith voltage vector group during the sampling period, and d_{ij} is the duty cycle of the jth voltage vector. The weighted error is obtained by calculating the duty cycle of all the vectors in the voltage vector group. Therefore, according to the optimization method of minimizing the root mean square (RMS) value of the weighted error within a voltage vector group, the RMS value of the weighted error for a given voltage vector group is [23]:

$$\mathcal{E}_{jRMS}^2 = \frac{1}{2}\sum_{i=1}^{2}(e_{ij}d_{ij})^2 = \overline{\mathcal{E}}_j^2 + \mathcal{E}_{j\sigma}^2 \quad (10)$$

$\mathcal{E}_{j\sigma}^2 = 1/2\sum_{i=1}^{2}(e_{ij}d_{ij} - \overline{\mathcal{E}}_j)^2$ is the variance of the weighted error, and the mean of the weighted error is defined as:

$$\overline{\mathcal{E}}_j = \frac{1}{2}\sum_{i=1}^{2} e_{ij}d_{ij} \quad (11)$$

Due to $e_{ij}d_{ij} \geq 0$, minimizing the effective value of $\mathcal{E}_j$ will result in the minimization of both the mean value $\overline{\mathcal{E}}_j$ and the standard deviation $\mathcal{E}_{j\sigma}$. Here, $\mathcal{E}_{j\sigma}$ is the effective value of the unbiased ripple in $\mathcal{E}_j$. Therefore, the duty cycle obtained by this method is calculated by minimizing the system constraints, and the duty cycle of each vector in the group of voltage vectors can be calculated from the following equation:

$$\min_{d_j} G_j = \frac{1}{2}\sum_{i\in\mathcal{R}_j} e_{ij}^2 d_{ij}^2 = \frac{1}{2}\sum_{i\in\mathcal{R}_j} g_{ij} d_{ij}^2$$
$$\text{s.t.} \quad \sum_{i\in\mathcal{R}_j} d_{ij} = 1 \; (0 \leq d_{ij} \leq 1, \; \forall i \in \mathcal{R}_j) \quad (12)$$

The optimization problem can be solved with the help of the Lagrange Multiplier Method. Since the solution satisfies the Karush-Kuhn-Tucker condition, and (12) represents a convex function, the solution is optimal and is obtained:

$$d_{ij} = \frac{Q_j}{g_{ij}}, \quad Q_j = \frac{1}{\sum_{i\in\mathcal{R}_j} g_{ij}^{-1}} \quad (13)$$

The role of Q_j is to ensure that the sum of the duty cycles of the vectors in the group of voltage vectors is equal to 1. At the same time, there is always a feasible solution to (13), i.e., $0 \leq d_{ij} \leq 1$. In addition, for each group of vectors in (13), a set of local minima solutions is obtained.

3.3. DV-M^{2}PC Strategy

The FCS-MPC strategy employs only one effective vector, which means that the direction of the final voltage vector will be limited to the direction of the six effective vectors. Based on the eight basic voltage vectors, 12 voltage vector combinations $u_{mi}(u_j, u_k)$ as shown in Figure 5 are defined. They are combinations of effective and zero vectors: $u_{m1}(u_0, u_1)$, $u_{m2}(u_7, u_2)$, $u_{m3}(u_0, u_3)$, $u_{m4}(u_7, u_4)$, $u_{m5}(u_0, u_5)$, $u_{m6}(u_7, u_6)$, and combinations of effective and effective vectors: $u_{m7}(u_1, u_2)$, $u_{m8}(u_2, u_3)$, $u_{m9}(u_3, u_4)$, $u_{m10}(u_4, u_5)$, $u_{m11}(u_5, u_6)$, $u_{m12}(u_6, u_1)$. Based on the principle of volt-second balance, the synthesized voltage vector is expressed by the double-vector voltage combination as:

$$u_{mi} = d_{i,uj}u_j + d_{i,uk}u_k \quad (14)$$

where $d_{i,uj}$ and $d_{i,uk}$ are the duty cycles of u_j and u_k, respectively, and $d_{i,uj} + d_{i,uk} = 1$. Since it is also needed to calculate the capacitor voltage under the resynthesized voltage vector, it

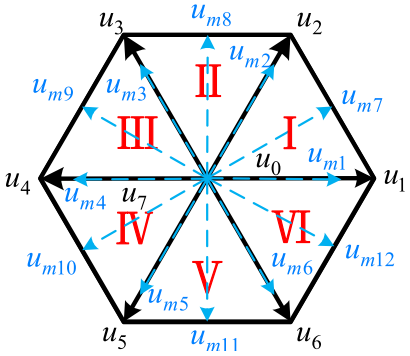

FIGURE 5. Vector diagram of the DV-M^{2}PC strategy.

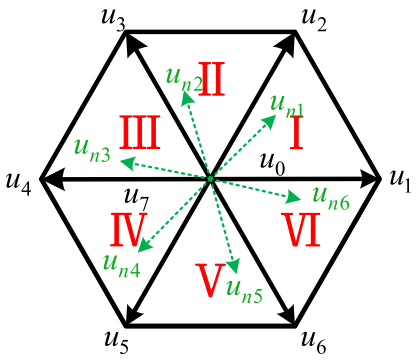

FIGURE 6. Vector diagram of TV-M^{2}PC strategy.

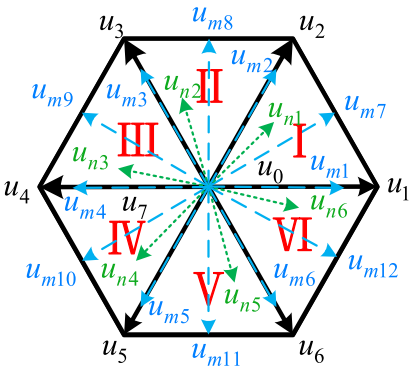

FIGURE 7. Vector diagram of DTVH-M^{2}PC strategy.

is calculated as:

$$u_{C1} = u_{C1(uj)} \times d_{i,uj} + u_{C1(uk)} \times d_{i,uk} \tag{15}$$

where $u_{C1(uj)}$ and $u_{C1(uk)}$ are the capacitance voltages under the action of u_j and u_k voltage vectors, respectively. $u_{C1(uj)}$ and $u_{C1(uk)}$ can be obtained according to the capacitance voltage calculation formula in the NST state. The duty cycle of voltage vectors is derived according to (13):

$$\begin{cases} d_{i,uj} = \frac{g_{uk}}{g_{uj}g_{uk}} \\ d_{i,uk} = \frac{g_{uj}}{g_{uj}g_{uk}} \end{cases} \tag{16}$$

where g_{uj} and g_{uk} are the value functions obtained by substituting u_j and u_k into (8), respectively. In order to realize the DV-M^{2}PC strategy, firstly the vector duty cycle should be calculated. Then, the voltage vector and capacitor voltage values synthesized from the 12 voltage vector groups are obtained using (14) and (15). Finally, by substituting (8), the switching state with the smallest cost function value is selected for input to the inverter.

3.4. TV-M^{2}PC Strategy

Although double-vector improves the control performance of single-vector, it still suffers from many harmonic disturbances and low output quality. Therefore, to address these issues, at least two effective vectors and one zero vector need to be employed. The TV-M^{2}PC uses three fundamental voltage vectors in each control cycle and can define six voltage vector combinations $u_{ni}(u_j, u_k, u_l)$ as shown in Figure 6 is defined, namely $u_{n1}(u_0, u_1, u_2)$, $u_{n2}(u_0, u_2, u_3)$, $u_{n3}(u_0, u_3, u_4)$, $u_{n4}(u_0, u_4, u_5)$, $u_{n5}(u_0, u_5, u_6)$ and $u_{n6}(u_0, u_6, u_7)$. Similarly, the synthesized voltage vector is represented by the combination of three voltage vectors as follows:

$$u_{ni} = d_{i,uj}u_j + d_{i,uk}u_k + d_{i,ul}u_l \tag{17}$$

where $d_{i,uj}$, $d_{i,uk}$, and $d_{i,ul}$ are the duty cycles of u_j, u_k, and u_l, respectively, and $d_{i,uj} + d_{i,uk} + d_{i,ul} = 1$. Similarly, the capacitor voltage is calculated as:

$$u_{C1} = u_{C1(uj)} \times d_{i,uj} + u_{C1(uk)} \times d_{i,uk} + u_{C1(ul)} \times d_{i,ul} \tag{18}$$

where $u_{C1(uj)}$, $u_{C1(uk)}$, and $u_{C1(u_l)}$ are the capacitance voltage values under the action of u_j, u_k, and u_l voltage vectors, respectively. And the same is calculated according to the capacitance voltage calculation formula in the NST state. The duty cycle of voltage vectors is deduced from (14) for each in the group of voltage vectors:

$$\begin{cases} d_{i,uj} = \frac{1/g_{uj}}{1/g_{uj}+1/g_{uk}+1/g_{ul}} \\ d_{i,uk} = \frac{1/g_{uk}}{1/g_{uj}+1/g_{uk}+1/g_{ul}} \\ d_{i,ul} = \frac{1/g_{ul}}{1/g_{uj}+1/g_{uk}+1/g_{ul}} \end{cases} \tag{19}$$

where g_{uj}, g_{uk}, and g_{ul} are the value functions obtained by substituting u_j, u_k, and u_l into (8), respectively. In order to realize the TV-M^{2}PC strategy, firstly the vector duty cycle should be calculated, then by using (17) and (18), the voltage vectors and capacitor voltages are obtained by combining the six voltage vectors, and finally, by substituting (8), the switching state with the smallest cost function value is selected for input to the inverter.

3.5. DTVH-M^{2}PC Strategy

The double-vector control strategy has a smaller switching frequency, while the triple-vector control strategy has a better steady-state performance. So when only the DV-M^{2}PC or TV-M^{2}PC strategy is used, the optimal control cannot be realized yet. To minimize the control error, a DTVH-M^{2}PC strategy is further proposed, which combines the DV-M^{2}PC and TV-M^{2}PC strategies, and a fast selection table of vector combinations is used to reduce the computational effort.

The DTVH-M^{2}PC strategy selects the optimal voltage vectors by evaluating the cost function of 18 voltage vectors. These 18 voltage vector sets are shown in Figure 7, including 12 voltage vector sets (u_{m1}-u_{m12}) synthesized from two voltage vectors shown in Figures 5 and 6 voltage vector sets (u_{n1}–u_{n6}) synthesized from three voltage vectors shown in Figure 6. The method of calculating the vector duty cycle for the 12 voltage vector combinations (u_{m1}-u_{m12}) and 6 voltage vector combinations (u_{n1}-u_{n6}) is the same as that for the DV-M^{2}PC and TV-M^{2}PC strategies. In the computation of the DTVH-M^{2}PC strategy, 18 voltage vector combinations are first evaluated in each sampling cycle, and then the optimal voltage vector is determined by (8) and input to the inverter.

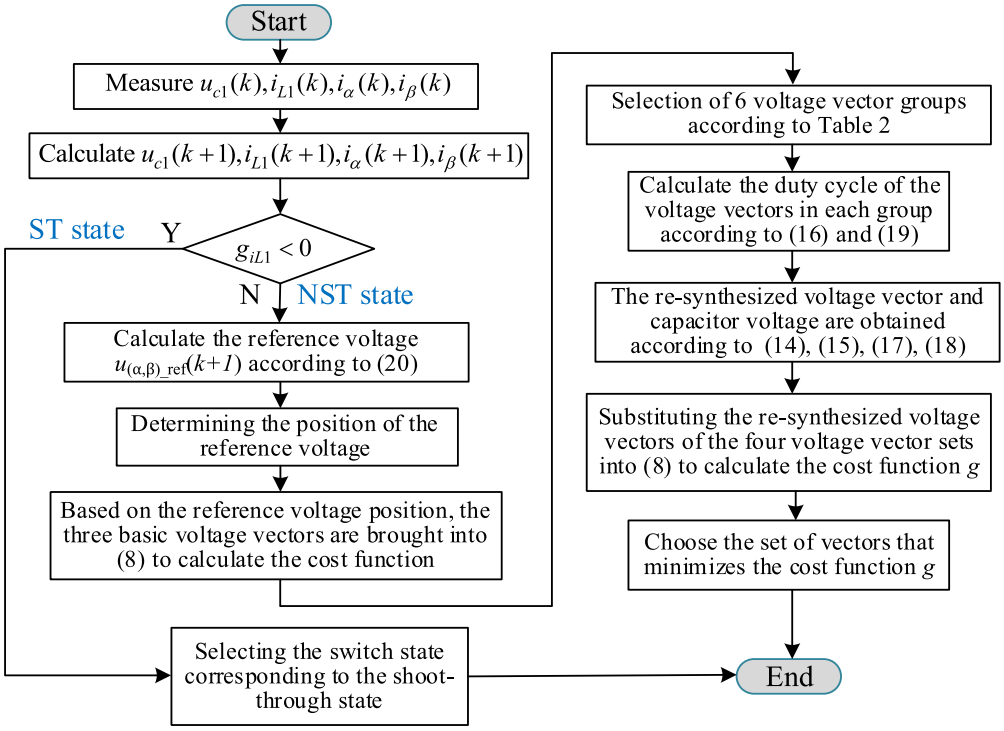

FIGURE 8. Algorithm flowchart.

Since the DTVH-M^{2}PC strategy has 18 sets of voltage vectors, its computation is large. In order to reduce its calculation amount, it needs to be simplified. Based on the principle of deadbeat control and combined with (2), the future output voltage (reference voltage) is derived:

$$u_{(\alpha,\beta)\_ref}(k+1) = \frac{L\left[i_{(\alpha,\beta)\_ref}(k+1) - i_{(\alpha,\beta)}(k)\right]}{T} + Ri_{(\alpha,\beta)}(k+1) + e_{(\alpha,\beta)}(k+1) \quad (20)$$

Table 2 is then utilized to derive the position of the reference voltage, where $\theta = \arctan(u_{\beta\_ref}/u_{\alpha\_ref})$. The cost function can then be calculated by substituting the three basic voltage vectors into (8) according to the position of the reference voltage. When the reference voltage is in sector I, the cost functions of $u_0(u_7), u_1, u_2, u_3$ and u_6 should be calculated only, and then six combinations of voltage vectors are preselected, with voltage vector combinations of u_{m1}, u_{m2}, u_{m7}, u_{n1}, u_{n2}, and u_{n6}.

TABLE 2. Sector of reference voltage and quick selection of voltage vector combinations.

Sector	Angular range of θ	Voltage vector combination selection
I	$[0, \pi/3)$	$u_{m1}, u_{m2}, u_{m7}, u_{n1}, u_{n2}, u_{n6}$
II	$[\pi/3, 2\pi/3)$	$u_{m2}, u_{m3}, u_{m8}, u_{n1}, u_{n2}, u_{n3}$
III	$[2\pi/3, \pi)$	$u_{m3}, u_{m4}, u_{m9}, u_{n2}, u_{n3}, u_{n4}$
IV	$[\pi, 4\pi/3)$	$u_{m4}, u_{m5}, u_{m10}, u_{n3}, u_{n4}, u_{n5}$
V	$[4\pi/3, 5\pi/3)$	$u_{m5}, u_{m6}, u_{m11}, u_{n4}, u_{n5}, u_{n6}$
VI	$[5\pi/3, 2\pi)$	$u_{m6}, u_{m1}, u_{m12}, u_{n1}, u_{n5}, u_{n6}$

The above algorithm not only ensures the desired output current and voltage control performance in one control cycle, but also reduces the 18 groups of voltage vectors that need to be computed to 6 groups, which greatly reduces the computation amount without decreasing the control performance, and the overall implementation process of the proposed strategy is used as shown in Figure 8. Compared with the DV-M^{2}PC and TV-M^{2}PC strategies, the DTVH-M^{2}PC strategy has a richer set of voltage vectors, which fully compares different voltage vectors, and the control performance is further improved.

To achieve the overall control of the qZSI-VSG system, the control structure is shown in Figure 9. The overall control of the qZSI-VSG system is realized by firstly calculating the system power through the sampled three-phase output currents and voltages, then providing the reference voltage value and phase angle through the active and reactive power control of the VSG, then realizing the decoupling of active and reactive powers through the virtual impedance control [24], and finally selecting the optimal switching state to be applied to the inverter using the MPC control.

4. EXPERIMENTAL ANALYSIS

To validate the feasibility and efficacy of the proposed strategy, an experimental model is constructed on the RT-LAB hardware experimental platform, and the experimental platform of the system is shown in Figure 10. TMS320F2812 is selected as the model of the DSP controller. The model system parameters are shown in Table 3, and this paper verifies the model performance in both steady-state and perturbation experiments, respectively.

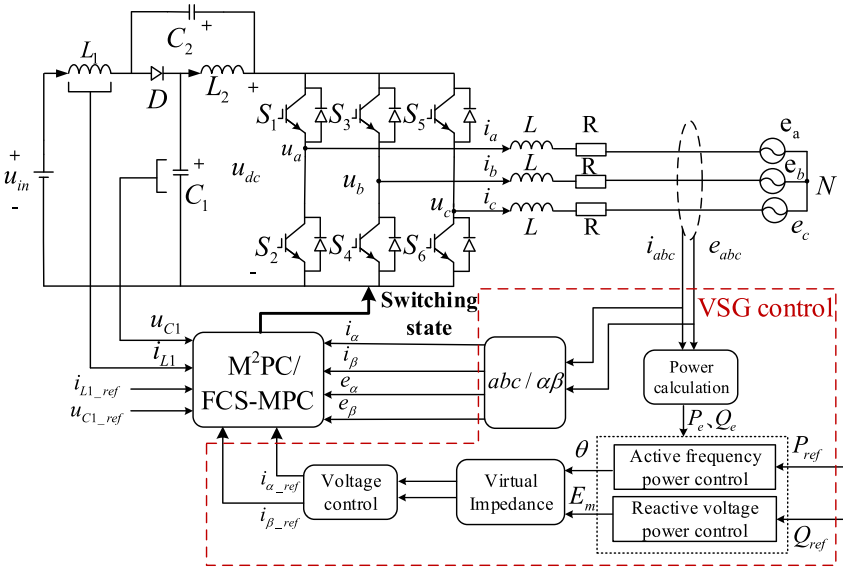

FIGURE 9. System overall control block diagram.

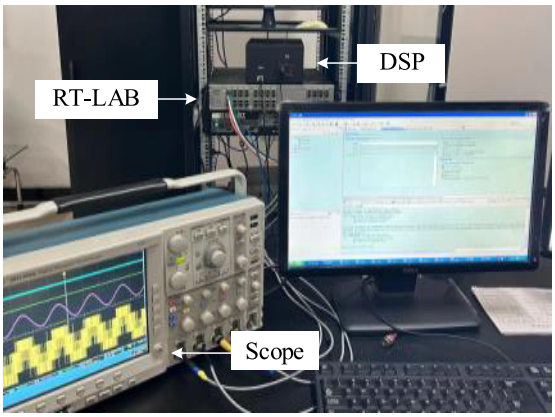

FIGURE 10. RT-LAB experiment platform.

Parameters	Values
Input voltage (V_{in})	225 V
Grid line voltage (e)	380 V
qZSI inductance (L_1, L_2)	4 mH
qZSI capacitance (C_1, C_2)	220 μF
Filter inductors (L)	4 mH
Rotational inertia (J)	0.2 kg·m^2
Damping factor (D)	30 N·m·s/rad
Sampling period (T_s)	25 μS
Grid frequency (f)	50 Hz
Integrator gain (k_i)	3
Reactive voltage sag coefficient (k_q)	350

TABLE 3. QZSI-VSG system parameters.

4.1. Steady-State Operation

To evaluate control performance in steady-state conditions, the input voltage of the system is set to 225 V, and the output power reference is fixed at 2000 W. Figure 11 illustrates a comparison of the DV-M^{2}PC, TV-M^{2}PC, DTVH-M^{2}PC, and conventional FCS-MPC strategies during this steady-state operation. The waveforms displayed from top to bottom represent the inductor current i_{L1}, capacitance voltage u_{C1}, A-phase output current i_A, and A-phase output voltage U_A. It is seen that under the DV-M^{2}PC strategy, the TV-M^{2}PC strategy and DTVH-M^{2}PC strategy, both the inductor current and capacitor voltage still track their reference values accurately, and stable capacitor voltage u_{c1} is obtained. It shows that the effectiveness of the proposed method is comparable to that of the traditional FCS-MPC strategy, thus confirming the validity of the strategy outlined in this paper. Because the DTVH-M^{2}PC strategy has a larger selectable range of output voltage vectors, the control accuracy for capacitor voltage is higher. The experimental results show that the DTVH-M^{2}PC, TV-M^{2}PC, and DV-M^{2}PC strategies reduce the capacitive voltage ripple by 25.53%, 20.92% and 13.12%, respectively, compared with the FCS-MPC strategy.

Figure 12 shows the current spectrum analysis plots for FCS-MPC, DV-M^{2}PC, TV-M^{2}PC, and DTVH-M^{2}PC strategies. The current THD under the conventional FCS-MPC strategy is 5.80%, which does not satisfy the grid connection requirements. Because the conventional control strategy selects only one vector in a cycle, the final synthesized vectors are limited to the directions of the six effective voltage vectors. Multi-vector control systems employing at least two effective vectors and one zero vector are richer in voltage vectors than single-vector control, and the DTVH-M^{2}PC strategy, which combines the advantages of the two multi-vectors, achieves better control results. Compared with the FCS-MPC strategy, the DV-M^{2}PC, TV-M^{2}PC, and DTVH-M^{2}PC strategies, with current THD of 4.59%, 3.66%, and 2.98%, respectively, fully satisfy the grid-connected requirements, achieve better output harmonic performance, and improve the control accuracy of the system current.

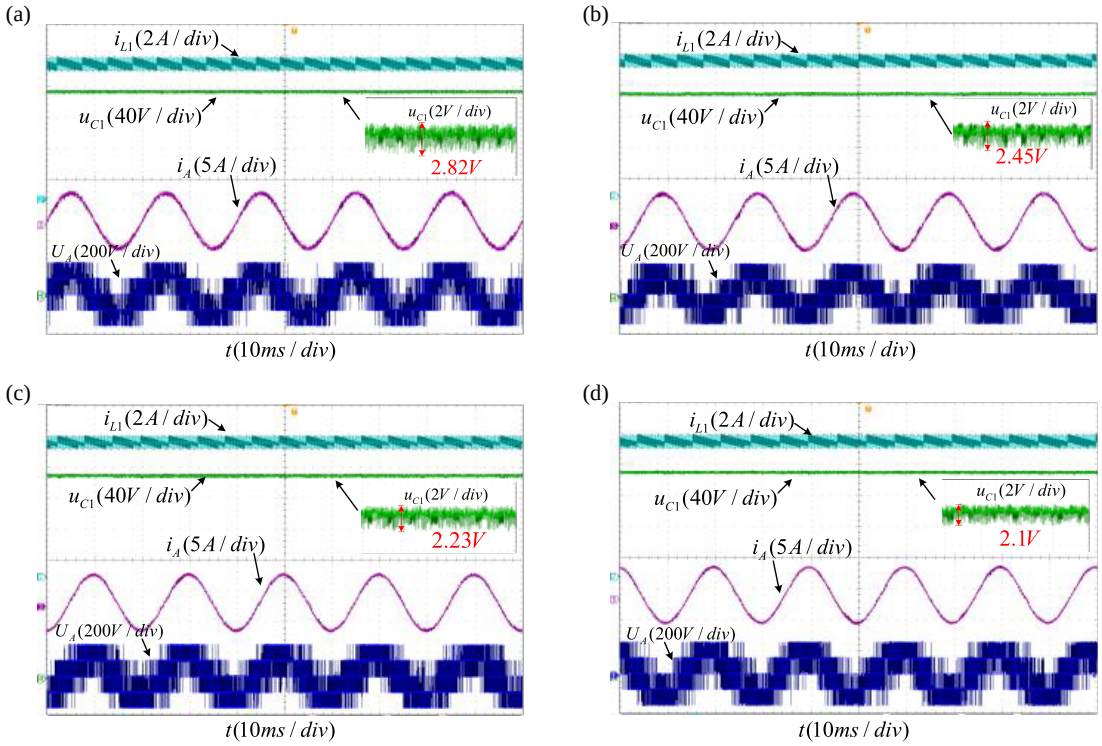

FIGURE 11. Experimental waveforms of steady-state operation. (a) FCS-MPC. (b) DV-M^{2}PC. (c) TV-M^{2}PC. (d) DTVH-M^{2}PC.

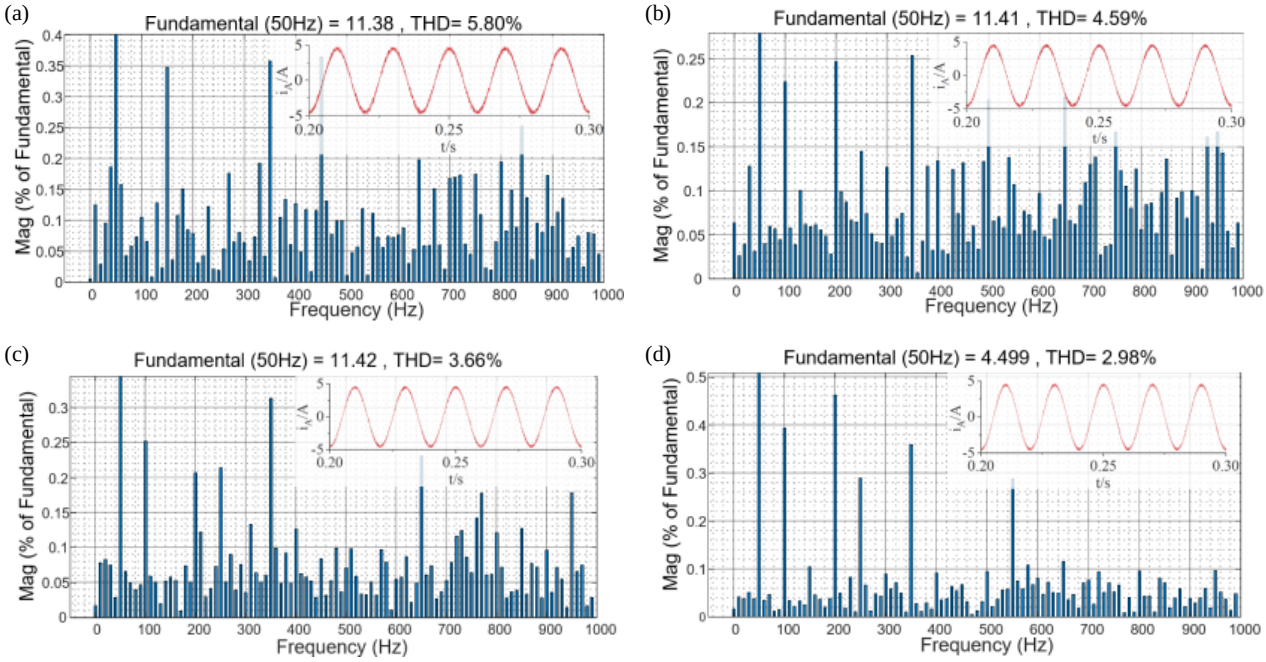

FIGURE 12. Current spectrum analysis. (a) FCS-MPC. (b) DV-M^{2}PC. (c) TV-M^{2}PC. (d) DTVH-M^{2}PC.

To verify the effectiveness of the DTVH-M^{2}PC strategy for qZSI control, Figure 13 gives a localized and enlarged view of the experimental waveforms of the capacitor voltage u_{C1}, inductor current i_{L1}, and dc chain voltage u_{dc}. When the ST vector is selected, the inductor current rises; the DC side bus voltage drops to zero; and the capacitor voltage falls. When the NST vector is selected, the inductor current falls; the DC chain voltage rises to u_{dc}; and the capacitor voltage rises to the set value and then maintains constant. From the above steady-state performance experiments, it can be seen that the DV-M^{2}PC, TV-M^{2}PC, and DTVH-M^{2}PC strategies can achieve the control objectives, and the DTVH-M^{2}PC strategy has better steady-state performance, smaller total harmonic distortion of the output current, and smaller capacitor voltage ripple.

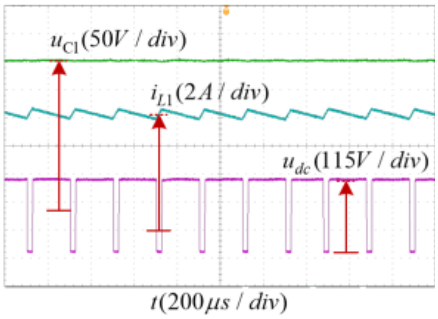

FIGURE 13. Detailed presentation of experimental results under the DTVH-M^{2}PC strategy.

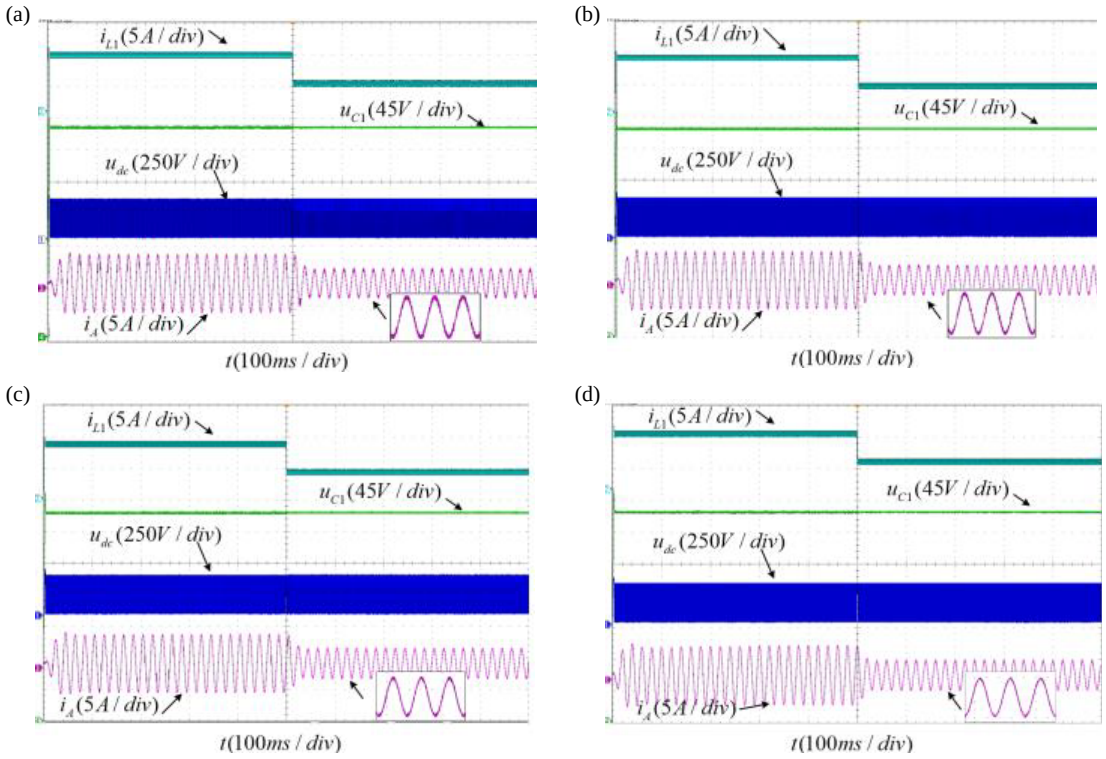

FIGURE 14. Experimental waveform of output power 2000 W step to 1000 W. (a) FCS-MPC. (b) DV-M^{2}PC. (c) TV-M^{2}PC. (d) DTVH-M^{2}PC.

4.2. Reference Output Power Step Change

To qualitatively analyze the stability of the qZSI-VSG system, reference output power perturbation test experiments are given for the FCS-MPC, DV-M^{2}PC, TV-M^{2}PC, and DTVH-M^{2}PC strategies. Keeping the DC input voltage u_{in} constant at 225 V and the DC chain voltage u_{dc} constant at 300 V, the reference output power P_{o_ref} is stepped from 2000 W to 1000 W. The experimental waveforms from top to bottom in Figure 14 are the inductor current i_{L1}, capacitor voltage u_{C1}, DC chain voltage u_{dc}, and A-phase output current i_A, respectively. Regardless of which strategy is used, when the output power disturbance occurs, the inductor current decreases; the peak output phase current decreases to a given value within 0.1 s; and the capacitor voltage remains constant. The aforementioned four strategies effectively attain precise tracking control of output power disturbance, thereby guaranteeing the system's stability and reliability under the given operational circumstances. Consistent with the analytical results in the steady state experiments, among these four strategies, the FCS-MPC strategy has the largest output current harmonics, and the DTVH-M^{2}PC strategy has the smallest output current harmonics. The DTVH-M^{2}PC strategy not only has the smallest current harmonic but also can achieve comparable control effects with the FCS-MPC method. In addition, the output power variation has a lower effect on the current harmonic of DTVH-M^{2}PC.

Figure 15 shows the experimental waveforms of active power P and reactive power Q under the step change of the output power of FCS-MPC and DV-M^{2}PC, TV-M^{2}PC, and DTVH-M^{2}PC strategies. The decoupling of active and reactive power is realized by adding the virtual impedance in the VSG control, so that it is seen that the active power has the inertia and damping and can follow the change of the power command well, and the reactive power is approximated to the set value 0 var. From the experimental result, the DTVH-M^{2}PC, TV-M^{2}PC, and DV-M^{2}PC strategies reduce the active power ripple by 50%, 37.93% and 22.41% and the reactive power ripple by 62.85%, 40%, and 25.71%, respec-

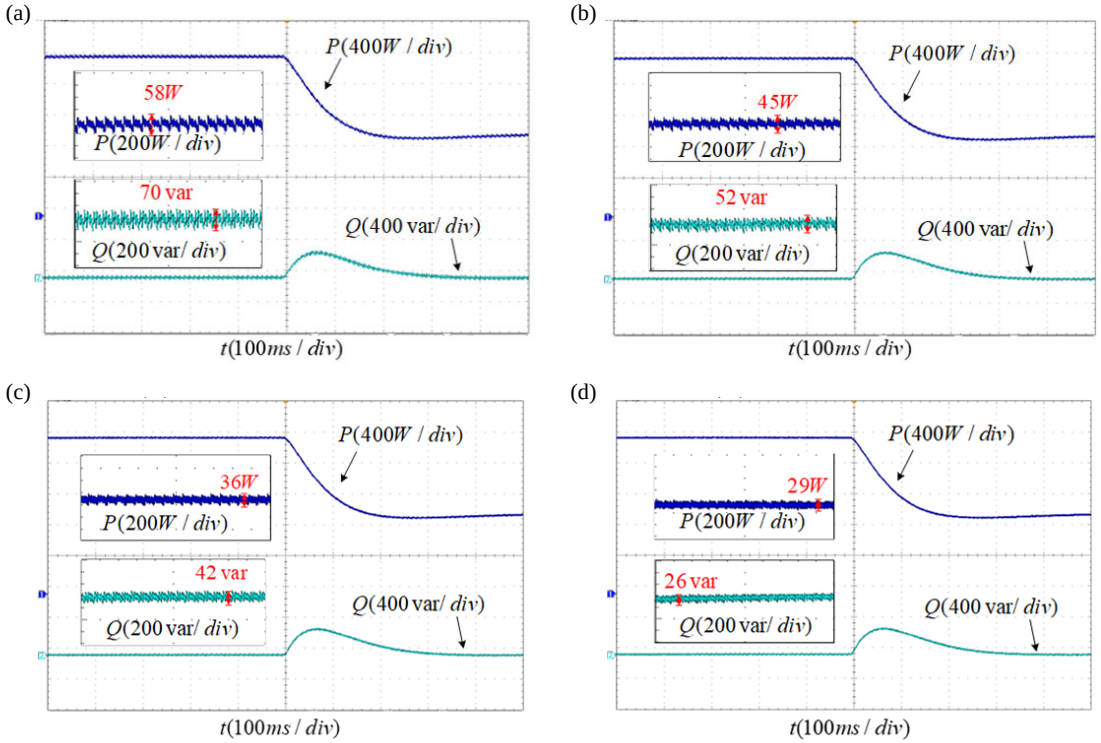

FIGURE 15. Experimental waveforms of active and reactive power at output power 2000 W step to 1000 W. (a) FCS-MPC. (b) DV-M^{2}PC. (c) TV-M^{2}PC. (d) DTVH-M^{2}PC.

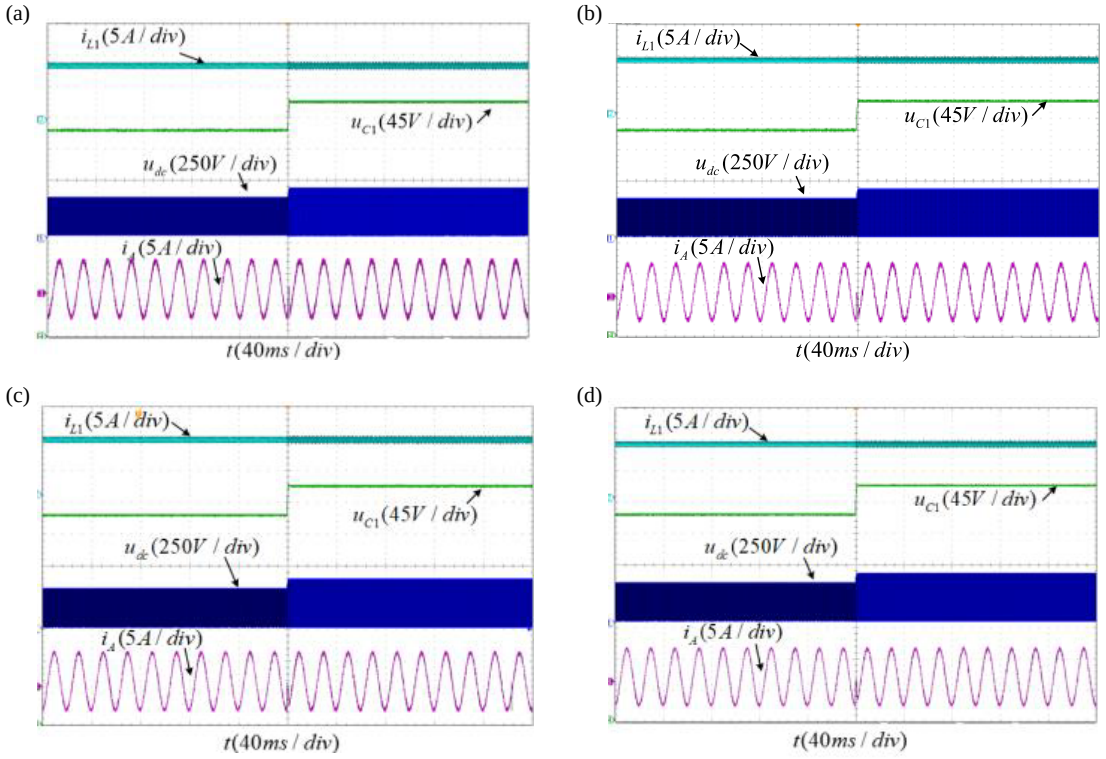

FIGURE 16. Experimental waveform of DC chain voltage 300 V step to 375 V. (a) FCS-MPC. (b) DV-M^{2}PC. (c) TV-M^{2}PC. (d) DTVH-M^{2}PC.

tively, compared to the FCS-MPC strategy. This is due to the inaccuracy of the single-vector based FCS-MPC in selecting the vectors leading to its low control accuracy. In contrast, the DTVH-M^{2}PC strategy proposed in this paper can effectively reduce the power ripple, which indicates that compared with the FCS-MPC strategy, the DTVH-M^{2}PC strategy proposed in

this paper is more accurate in vector selection and therefore has higher control accuracy, which verifies the effectiveness of the strategy.

To summarize, the DTVH-M^{2}PC strategy has smaller power ripple and output current harmonic with higher control accuracy than the other three strategies with no difference in transient performance.

4.3. DC Chain Voltage Step Change

In the qualitative analysis of the system stability in the DC chain voltage perturbation experiment, the DC input voltage is kept constant at 225 V; the reference output power is kept constant at 2000 W; and the experimental waveforms of the step change of the DC chain voltage are shown in Figure 16 when the DC chain voltage, u_{dc} rises from 300 V to 375 V. When the DC chain voltage increases, the capacitor voltage also increases, and the output current remains constant. The output current quickly tends to a steady-state after a short oscillation, and the capacitor voltage and DC chain voltage waveforms quickly follow their reference values. Compared with the FCS-MPC strategy, the DTVH-M^{2}PC strategy has better output current waveforms when DC chain voltage is changed, and each control variable follows its reference value better, while ensuring good transient performance.

5. CONCLUSION

In this paper, a DTVH-M^{2}PC strategy for qZSI-VSG system is proposed for the issue of large output current harmonic and power ripple, and the following conclusions are drawn through experimental verification:

1) In the DV-M^{2}PC and TV-M^{2}PC strategies, the duty cycle of the voltage vector is calculated by the inverse relationship between the duty cycle and the value of the cost function, which realizes the control of multi-objects under the multi-vector control strategy and ensures the control performance for multi-objects.

2) By combining the DV-M^{2}PC and TV-M^{2}PC strategies, the proposed DTVH-M^{2}PC strategy reduces 48.62% of the output current harmonic, 50% of the active power ripple, and 25.53% of the capacitor voltage ripple compared with that of the FCS-MPC strategy without weakening the transient performance of the FCS-MPC strategy, which effectively improves the system control performance.

3) The DTVH-M^{2}PC strategy effectively reduces the computational effort by reducing the voltage vector groups from 18 to 6 through the vector combination quick selection table.

ACKNOWLEDGEMENT

This work was supported by the Natural Science Foundation of Hunan Province of China under Grant Number 2023JJ50191.

REFERENCES

[1] Yang, X.-Z., J.-H. Su, M. Ding, J.-W. Li, and Y. Du, "Control strategy for virtual synchronous generator in microgrid," in *2011 4th International Conference on Electric Utility Deregulation and Restructuring and Power Technologies (DRPT)*, 1633–1637, Weihai, China, Jul. 2011.

[2] Xu, H., "Research on generalized inertia and reactive power sharing strategy of VSG," Ph.D. dissertation, Hefei University of Technology, Hefei, China, 2017.

[3] Visscher, K. and S. W. H. D. Haan, "Virtual synchronous machines (VSG's) for frequency stabilisation in future grids with a significant share of decentralized generation," in *CIRED Seminar 2008: SmartGrids for Distribution*, 1–4, Frankfurt, Germany, Jun. 2008.

[4] Peng, F. Z., "Z-source inverter," *IEEE Transactions on Industry Applications*, Vol. 39, No. 2, 504–510, Mar.–Apr. 2003.

[5] Wang, Z., Y. Guo, Y. Guo, *et al.*, "Quasi Z-source six-leg voltage-source inverter based on a new space vector modulation strategy," *Power System Protection and Control*, Vol. 46, No. 21, 45–54, Nov. 2018.

[6] Liu, C., X. Tian, Y. Wang, G. Cai, and X. Tian, "Single-phase multi-cell voltage source inverter," *Transactions of China Electrotechnical Society*, Vol. 32, No. 24, 8–96+114, Nov. 2017.

[7] Anderson, J. and F. Z. Peng, "Four quasi-Z-source inverters," in *2008 IEEE Power Electronics Specialists Conference*, 2743–2749, Rhodes, Greece, Jun. 2008.

[8] Cheema, K. M. and K. Mehmood, "Improved virtual synchronous generator control to analyse and enhance the transient stability of microgrid," *IET Renewable Power Generation*, Vol. 14, No. 4, 495–505, 2020.

[9] Feng, J., F. Bai, M. Nadarajah, and H. Ma, "Transition towards inverter-based generation with VSG control: Low frequency instability prospective," in *2023 IEEE International Conference on Energy Technologies for Future Grids (ETFG)*, 1–6, Wollongong, Australia, Dec. 2023.

[10] Vazquez, S., J. I. Leon, L. G. Franquelo, J. Rodriguez, H. A. Young, A. Marquez, and P. Zanchetta, "Model predictive control: A review of its applications in power electronics," *IEEE Industrial Electronics Magazine*, Vol. 8, No. 1, 16–31, Mar. 2014.

[11] Rodriguez, J., M. P. Kazmierkowski, J. R. Espinoza, P. Zanchetta, H. Abu-Rub, H. A. Young, and C. A. Rojas, "State of the art of finite control set model predictive control in power electronics," *IEEE Transactions on Industrial Informatics*, Vol. 9, No. 2, 1003–1016, May 2013.

[12] Mosa, M., R. S. Balog, and H. Abu-Rub, "High-performance predictive control of quasi-impedance source inverter," *IEEE Transactions on Power Electronics*, Vol. 32, No. 4, 3251–3262, Apr. 2017.

[13] Bakeer, A., M. A. Ismeil, and M. Orabi, "A powerful finite control set-model predictive control algorithm for quasi Z-source inverter," *IEEE Transactions on Industrial Informatics*, Vol. 12, No. 4, 1371–1379, Aug. 2016.

[14] Zheng, C., T. Dragičević, and F. Blaabjerg, "Model predictive control-based virtual inertia emulator for an islanded alternating current microgrid," *IEEE Transactions on Industrial Electronics*, Vol. 68, No. 8, 7167–7177, Aug. 2021.

[15] Chen, W., S. Zeng, G. Zhang, T. Shi, and C. Xia, "A modified double vectors model predictive torque control of permanent magnet synchronous motor," *IEEE Transactions on Power Electronics*, Vol. 34, No. 11, 11 419–11 428, Nov. 2019.

[16] Zhang, Y. and H. Yang, "Two-vector-based model predictive torque control without weighting factors for induction motor drives," *IEEE Transactions on Power Electronics*, Vol. 31, No. 2, 1381–1390, Feb. 2016.

[17] Zhang, Y., Y. Peng, and H. Yang, "Performance improvement of two-vectors-based model predictive control of PWM rectifier," *IEEE Transactions on Power Electronics*, Vol. 31, No. 8, 6016–

6030, Aug. 2016.

[18] Lan, Z., B. Wang, C. Xu, and L. Li, "A novel three-vector model predictive current control for permanent magnet synchronous motor," *Proceedings of the CSEE*, Vol. 38, No. S1, 243–249, 2018.

[19] Tarisciotti, L., P. Zanchetta, A. Watson, S. Bifaretti, and J. C. Clare, "Modulated model predictive control for a seven-level cascaded H-bridge back-to-back converter," *IEEE Transactions on Industrial Electronics*, Vol. 61, No. 10, 5375–5383, Oct. 2014.

[20] Yeoh, S. S., T. Yang, L. Tarisciotti, C. I. Hill, S. Bozhko, and P. Zanchetta, "Permanent-magnet machine-based starter-generator system with modulated model predictive control," *IEEE Transactions on Transportation Electrification*, Vol. 3, No. 4, 878–890, Dec. 2017.

[21] Tarisciotti, L., J. Lei, A. Formentini, A. Trentin, P. Zanchetta, P. Wheeler, and M. Rivera, "Modulated predictive control for indirect matrix converter," *IEEE Transactions on Industry Applications*, Vol. 53, No. 5, 4644–4654, 2017.

[22] Tarisciotti, L., A. Formentini, A. Gaeta, M. Degano, P. Zanchetta, R. Rabbeni, and M. Pucci, "Model predictive control for shunt active filters with fixed switching frequency," *IEEE Transactions on Industry Applications*, Vol. 53, No. 1, 296–304, Jan.-Feb. 2017.

[23] Donoso, F., A. Mora, R. Cárdenas, A. Angulo, D. Sáez, and M. Rivera, "Finite-set model-predictive control strategies for a 3L-NPC inverter operating with fixed switching frequency," *IEEE Transactions on Industrial Electronics*, Vol. 65, No. 5, 3954–3965, May 2018.

[24] Zhang, H., S. Kim, Q. Sun, and J. Zhou, "Distributed adaptive virtual impedance control for accurate reactive power sharing based on consensus control in microgrids," *IEEE Transactions on Smart Grid*, Vol. 8, No. 4, 1749–1761, 2017.